Elucidating Silanol Removal in MFI Nanosized Zeolites Through Controlled Post-Synthesis Hydrothermal Treatments

Hugo Cruchade, Francesco Dalena, Eddy Dib, Abdelhafid Aitblal, Diogenes Honorato Piva, Aymeric Magisson, Svetlana Mintova

Elucidating Silanol Removal in MFI Nanosized Zeolites Through Controlled Post-Synthesis Hydrothermal Treatments

Hugo Cruchade,[a] Francesco Dalena,[a] Eddy Dib,[a] Abdelhafid Aitblal,[a] Diogenes Honorato Piva,[a] Aymeric Magisson,[a] Svetlana Mintova[a*]

[a]*Laboratoire Catalyse et Spectrochimie (LCS), Normandie University, ENSICAEN, CNRS,14050 Caen, France*

*Corresponding author: svetlana.mintova@ensicaen.fr

Abstract

The rational control of silanol groups is still an elusive dream in zeolite synthesis. To enhance our understanding of this phenomenon, we have performed various hydrothermal post-synthesis treatments on nanosized Silicalite-1 using sodium molybdate, sodium chloride, and ultrapure water to evaluate the alteration of silanol content. All treated samples exhibited a phase transition from orthorhombic to monoclinic confirmed by X-ray diffraction (XRD). Fourier-Transform Infrared (FTIR) and solid-state Nuclear Magnetic Resonance (NMR) spectroscopy showed a decrease in the concentration of silanol groups in the post treated samples. The treatment with sodium molybdate leads to the removal of approximately 98% of the silanol groups, while the samples treated with sodium chloride and ultrapure water showed a decrease of 90% and 20% respectively, compared to the parent silicalite-1. Additionally, the results from pyridine adsorption followed by FTIR show that the Parent-Silicalite-1 and the H_2O-Silicalite-1 samples contain a significant amount of defects, requiring 13.55 and 11.18 µmol, respectively, to saturate all the unsymmetrical bridging sites, while for the sample treated with sodium chloride only 1.07 µmol is needed to saturate all siloxane sites. In contrast, the treatment with sodium molybdate produced a free-defects zeolite. Molybdenum was found to contribute to the removal of both weak and strong hydrogen-bonded silanol groups through its insertion into the zeolite framework, while sodium played a significant role in condensing open bridges within the zeolite framework and removing less weak and strong hydrogen bonded silanol groups. This condensation of silanol groups seems to be facilitated by the polarization of silanol groups in presence of Na^+ promoting the formation of siloxy groups that eventually condense easily with adjacent SiOH groups, liberating water molecules during the activation process of the samples.

Keywords: Silanol groups, nanosized zeolites, defects removal.

Introduction

Since the discovery of Mobil-Five (MFI) zeolites in the late 1960s, studies aiming to deeply understand their complex structures continue to emerge because of the high importance of these materials in the chemical industry[1]. Silicalite-1 and ZSM-5 are two counterparts of the same MFI phase, corresponding to the purely siliceous and the aluminum-containing MFI zeolites, respectively[2]. A long-standing historical debate has centered on the space group adopted by both zeolites either as made, with the structure-directing agent (SDA) inside the pores, or calcined after the removal of the SDA[3–6]. Furthermore, these zeolites exhibit a structural symmetry transition (orthorhombic-to-monoclinic) when temperature changes[7] or when they are filled with different guest molecules[8–13]. A recent study has shown that this transition may also correlate with the symmetry of the SDA used[14]. Then, the flexibility of the zeolite framework plays a key role in determining the adoption of symmetry.

In all the studies cited above, two Bravais lattices are involved: orthorhombic (Pnma) and monoclinic ($P2_1/n$). The Pnma space group is characterized by three angles of 90° and 12 nonequivalent tetrahedral sites, while the monoclinic P21/n exhibits a deviation of one angle by less than one degree, resulting in 24 nonequivalent tetrahedral sites. According to our previous studies, treating nanosized silicalite-1 with sodium molybdate leads to a splitting of some XRD peaks, accompanied by the removal of silanol groups[15,16]. Other treatments found in the literature aim to fine-tune the concentration of silanol groups in zeolites through either physical or chemical methods[15,17–19]. Given the significant impact of silanol groups on the properties of zeolites such as hydrophobicity, thermal stability, acidity, and coke-trapping ability, the understanding and control of such defects is of great interest[20–22]. However, the understanding of such groups is far from trivial. In a recent study, we demonstrated the complex nature of silanol groups in zeolites using a combination of NMR, IR and DFT techniques, and categorized the silanols in four groups: isolated (non H-bonded), weakly, moderately, and strongly H-bonded[23]. Notably, the distribution of silanol groups was found to vary with the crystal size, raising questions about their reactivity and acidity. Using DFT calculations, we calculated the deprotonation energy of these groups considering several configurations of silanols and Brønsted acid sites and we have found that silanol groups cover a wide range of acidities, with some reaching deprotonation energies equivalent to strong acids[21]. This study shed light on the favorable functionalization of nanosized zeolites with metals compared to micron-sized zeolites[15,16]. Despite significant progress in recent years, achieving rational control of silanol groups remains an elusive goal in zeolite synthesis. We

previously reported that treating Silicalite-1 with sodium molybdate could heal silanol groups[24,25]. Although the obtained Silicalite-1 was free of defects and molybdenum was incorporated into the zeolite structure, the role of the different components present in the post-treatment solution including H_2O and Na^+ in healing silanol groups are still unclear. To deepen our understanding of this phenomenon, we have performed different hydrothermal post-synthesis treatments on nanosized Silicalite-1 using (i) ultrapure water (H_2O), (ii) water and sodium chloride (H_2O + Na^+), and (iii) water and sodium molybdate (H_2O + Na^+ + MoO_4^{2-}) to evaluate the alteration of silanol content. These treatments resulted in an orthorhombic-to-monoclinic phase transition as determined by X-Ray Diffraction (XRD), and different degrees of silanol groups removal, as confirmed by Nuclear Magnetic Resonance (NMR) and Fourier-transform infrared spectroscopy (FTIR) analyses.

Materials and methods

Synthesis of Parent MFI zeolite

Silicalite-1 zeolite (MFI type framework structure) was prepared from a precursor suspension with the following molar composition: 1 SiO_2: 0.28 TPAOH: 40 H_2O. In a typical synthesis, tetra-*n*-propylammonium hydroxide (TPAOH, 20 wt.% aqueous, Alfa Aesar) was first mixed in a polypropylene bottle with ultrapure water under magnetic stirring, followed by dropwise addition of tetraethyl orthosilicate (TEOS, 98%, Aldrich). The solution was kept at room temperature under magnetic stirring for 24 h, and then hydrothermally treated at 90 °C for 42 h. After the treatment, the solid product was recovered by centrifugation and washed with ultrapure water until the supernatant reached a pH of 7. The solid was dried overnight at 60 °C and then calcined at 550 °C for 5 h.

Post-treatments of the Parent MFI zeolite

The silicalite-1 zeolite was post-treated under hydrothermal conditions in the following solutions: (1) ultrapure Milli-Q water (18.2 MΩ.cm), (2) an aqueous solution of sodium chloride (NaCl, Alfa Aesar), and (3) an aqueous solution of sodium molybdate (Na_2MoO_4. $2H_2O$, Alfa Aesar). For both sodium molybdate and sodium chloride post-treatment, the aqueous solution was prepared by dissolving the appropriate amount of salt to achieve a sodium concentration of 0.3 mol L^{-1}. The parent Silicalite-1 was mixed with the post-treatment solution at a solid-to-liquid ratio of 1:20 in polypropylene bottles and stirred magnetically for 3 h at room temperature. The hydrothermal post-synthesis treatment was then carried out at 90°C for 7 days. The treated samples were washed with ultrapure water

and centrifugation. Finally, the solids were dried at 60 °C overnight and calcined at 550 °C for 5 h.

The prepared samples are abbreviated as follow: parent silicalite-1 sample is referred to as Parent-Silicalite-1, the sample treated with ultrapure water is referred as H_2O-Silicalite-1, the sample treated with an aqueous solution of sodium chloride is referred as Na-Silicalite-1, and sample treated with an aqueous solution of sodium molybdate is referred as Mo-Silicalite-1.

Characterization

X-ray diffraction (XRD) patterns were collected using a Bruker D8 Advance diffractometer equipped with Cu and Kα radiation (λ = 1.5418 Å) with a step of 0.017° at a scanning speed of 0.075 min^{-1}. Scanning Electron Microscopy (SEM) images and energy dispersive X-ray spectroscopy (EDS) analyses were performed using a JEOL JSM-IT800 Schottky field emission scanning electron microscope. SEM images were collected at low accelerating voltage of 0.8 keV and a current of 10 nA. EDS elemental analysis were acquired using an electron beam with a 10 keV. The particle sizes were measured with ImageJ software. ^{29}Si MAS NMR experiments were performed on Bruker AVANCE III (11.7 T) 500 MHz spectrometer at a resonance frequency of 99.3 MHz. The spectra were recorded with a 4 mm probe, spinning of 14 kHz. A $\pi/3$ pulse with a radiofrequency power of 21 kHz was applied, and a recycle delay of 20 s was used to ensure adequate relaxation between acquisitions. $\{^1H\}^{29}Si$ CP-MAS NMR cross-polarization experiments were performed with a contact time of 5 ms and a recycle delay of 2 s. The chemical shifts of ^{29}Si are referenced to tetramethylsilane (TMS).

Fourier transform infrared spectra (FT-IR) analysis of pyridine adsorbed were recorded by a Nicolet Nexus FTIR spectrophotometer. All spectra were recorded at 64 scans and a resolution of 4 cm^{-1}. The samples were pressed into self-supported disks with a radius of 1.6 cm and a weight of approximately 20 mg. Before the measurements, the disks were outgassed at 450 °C for 2 h under 10^{-6} torr pressure (heating rate of 5 °C min^{-1}). After saturating the sample with pyridine at room temperature, the sample was kept under vacuum (10^{-6} torr) for 30 minutes to remove physically adsorbed pyridine molecules. Spectra were acquired at 50, 100 and 150°C to estimate the desorption of pyridine. FT-IR spectra were post-processed using Peakfit software. The spectra were deconvoluted with Gaussian functions to better interpret and analyze specific wavenumbers. To ensure consistency of the obtained data, peak positions were constrained at specific wavenumber range, while amplitudes and widths were constrained. Subsequently, the software autonomously centered the Gaussians based on wavenumber, amplitudes, and widths to fit the spectrum trend in this region accurately, using

the appropriate number of functions. Furthermore, in order to elucidate the dynamic spectral behavior and analyze the impact of increasing the concentration of Py, the basic probe adsorption spectra were correlated using Two-Dimensional Correlation Spectroscopy (2D-COS)[26]. 2D-COS correlates changes in peak intensities induced by molecular perturbations, allowing the study of molecular behavior within the zeolites. This technique serves as a potent tool in analyzing different spectral datasets through the application of a cross-correlation function, yielding two distinct yet symmetrical 2D plots. The first plot, termed the synchronous plot, showcases positive peaks along the diagonal, known as auto peaks, summarizing the observed changes within the spectral dataset. This synchronous plot establishes relationships between spectral intensity changes that are in-phase with each other. Conversely, the second 2D plot, referred to as the asynchronous plot, delineates out-of-phase intensity changes, thereby enhancing resolution within the spectral region of interest. Distinguished from the synchronous plot by its lack of peaks along the diagonal, the asynchronous plot highlights spectral variations that occur with temporal or frequency offsets. Both plots exhibit off-diagonal peaks, known as cross peaks, which correlate spectral changes observed across the dataset. In our study, we employ 2D-COS to analyze the impact of increasing the mol number of Py, leveraging its ability to discern complex molecular interactions and elucidate dynamic spectral behavior.

Results and discussion

The SEM images of the Parent-Silicalite-1 sample with an average particle size of ~120 nm and the post-synthesis treated samples H_2O-Silicalite-1, Na-Silicalite-1, and Mo-Silicalite-1 are presented in **Figure 1**. As shown in **Figure 1A-D**, all the zeolite samples exhibit an irregular spherical morphology and no change is observed after the post-treatment. SEM-EDS elemental analysis shows an average Mo content of 0.26 wt% for the Mo-Silicalite-1 sample and a Na content of 0.13 wt% for the NaCl-Silicalite-1 sample (Table S1).

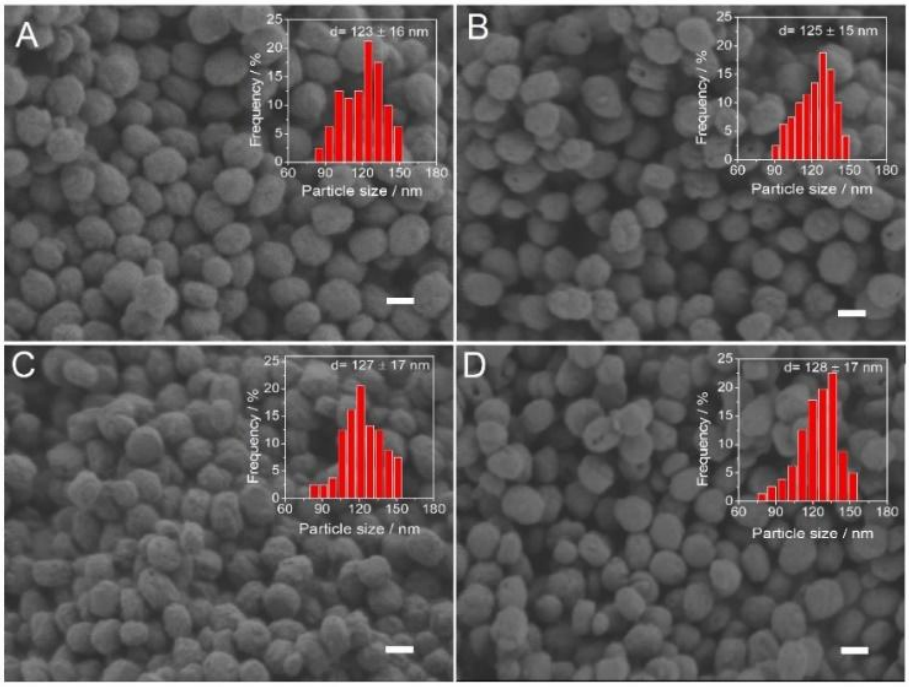

Figure 1. SEM images and particle size distribution (inset) of (A) Parent-Silicalite-1, (B) Mo-Silicalite-1, (C) Na-Silicalite-1 and (D) H_2O-Silicalite-1 samples.

The high crystallinity of the parent and post treated samples was confirmed by XRD (**Figure 2**). The Parent-Silicalite-1 sample exhibits orthorhombic symmetry (Pnma space group), while the post-synthesis treated samples showed the transition to the monoclinic symmetry. (Specifically, the splitting of the XRD peaks at 23.3°, 23.7°, and 24.4° (2θ) confirms the presence of the P21/n space group for both the Na-Silicalite-1 and Mo-Silicalite-1 samples. A more pronounced splitting was observed for samples Na-Silicalite-1 and Mo-Silicalite-1 (**Figure 2B**). This change is further corroborated by a clear variation in the unit cell volumes, calculated using Le Bail refinements in GSAS-II software[27]. The unit cell parameters and volumes for the Parent-, H_2 O-, Na-, and Mo-Silicalite-1 samples are detailed in **Table 1**. The increase in unit cell volume corresponds to expansions of 0.19, 0.26 and 0.27 % for samples H_2O-Silicalite-1, Mo-Silicalite-1 and Na-Silicalite-1, respectively, when compared to the Parent-Silicalite-1 sample.

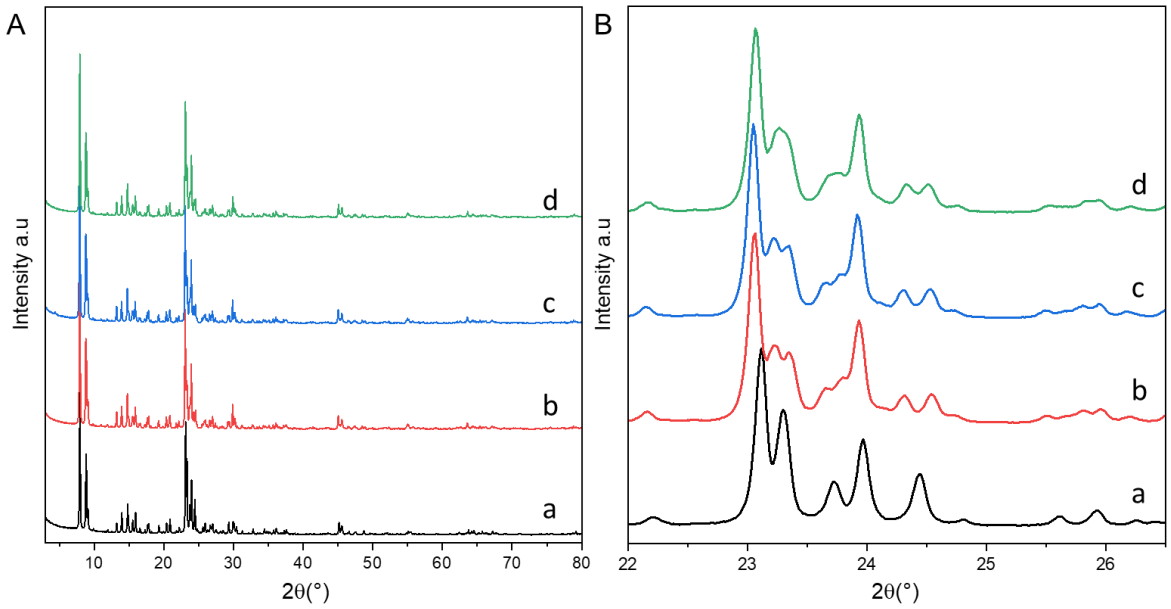

Figure 2. XRD patterns in the range of (A) 3 – 80° (2θ) and (B) and 22 – 27° (2θ) of (a) Parent-Silicalite-1, (b) Mo-Silicalite-1, (c) Na-Silicalite-1 and (d) H_2O-Silicalite-1 samples.

Table 1. Cell parameters and unit cell volume of the parent and post treated samples determined by Le Bail refinement.

Sample	Symmetry	a (Å)	b (Å)	c (Å)	β (°)	Volume (Å^3)	GOF	reduced X²	wR
Parent-Silicalite-1	Pnma	20.07459	19.89570	13.37975	-	5343.85	1.74	3.02	4.14
H_2O-Silicalite-1	$P2_1/n$	19.89701	20.10822	13.38301	90.5014	5354.25	1.70	2.90	4.09
Na-Silicalite-1	$P2_1/n$	19.89903	20.12017	13.38414	90.5915	5358.35	1.92	3.70	4.62
Mo-Silicalite-1	$P2_1/n$	19.89992	20.11966	13.38175	90.6089	5357.48	1.80	3.24	4.32

Considering the atomic-level ordering, ^{29}Si NMR spectra show a considerable enhancement in the spectral resolution of the Q^4 species, between -120 and -110 ppm, for Mo-Silicalite-1 and Na-Silicalite-1 (**Figure 3A**). This region corresponds to SiO_4 tetrahedra surrounded by four Si atoms[28]. The ^{29}Si chemical shifts are intimately related to Si-O-Si bond angles. The improved resolution indicates a higher degree of local order, as narrower angular distributions at the tetrahedral sites lead to more uniform chemical shift values. This enhanced order is not observed in the Parent-Silicalite-1 sample, and while the H_2 O-Silicalite-1 sample shows some spectral changes, the improvement in resolution is less pronounced. The slight reduction

in defect concentration in the H_2 O-Silicalite-1 sample suggests that the treatment had a minor effect, but not as significant as in the Mo- and Na-modified samples.

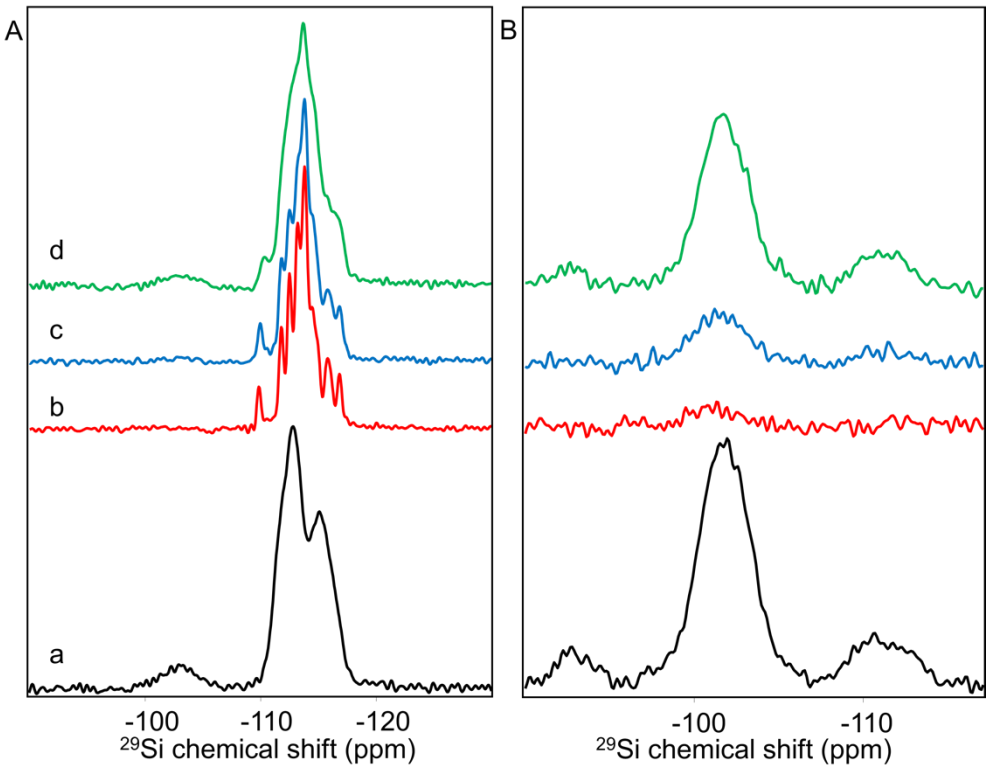

Figure 3. (A) Single pulse ^{29}Si NMR and (B) $^{29}Si\{^{1}H\}$ CPMAS NMR spectra of (a) Parent-Silicalite-1, (b) Mo-Silicalite-1, (c) Na-Silicalite-1 and (a) H_2O-Silicalite-1 samples.

The post-treatments have strongly influenced the local order of the crystals in all treated samples. To evaluate the concentration and nature of silanol groups, $^{29}Si\{^{1}H\}$ cross-polarization magic angle spinning NMR (CPMAS) spectra were recorded (**Figure 3B**). The main signal, centered at around -102 ppm corresponds to Q^3 species i.e. SiO_4 tetrahedra surrounded by three Si atoms and a hydrogen atom. This explains their selective detection in the CPMAS spectra, even though some Q^4 species appearing at -110 ppm may be in close vicinity to some silanols. A very low amount of Q2 species is observed at around -93 ppm, which corresponds to SiO_4 tetrahedra surrounded by two Si atoms and 2 hydrogen atoms. Based on the normalized intensities, the post-treatments seem to contribute to removing the silanol groups differently in the four treatments. The zeolite structure with fewest silanol groups is Mo-Silicalite-1, followed by Na-Silicalite-1 and H_2O-Silicalite-1. This correlates well with the improved resolution observed in the single pulse NMR spectra (**Figure 3A)**.

The amount and type of silanols groups of the samples have been studied by FTIR spectroscopy. The FTIR spectra (**Figure 4**) contain several bands in the hydroxyl region,

which can be categorized as follows: isolated and weakly hydrogen-bonded SiOH groups appear in the range of 3750–3735 cm^{-1}, SiOH groups influenced by medium-strength hydrogen bonding are observed between 3650–3500 cm^{-1}, and those affected by strong hydrogen bonding are found in the 3580–3300 cm^{-1} range[19,23,29] .

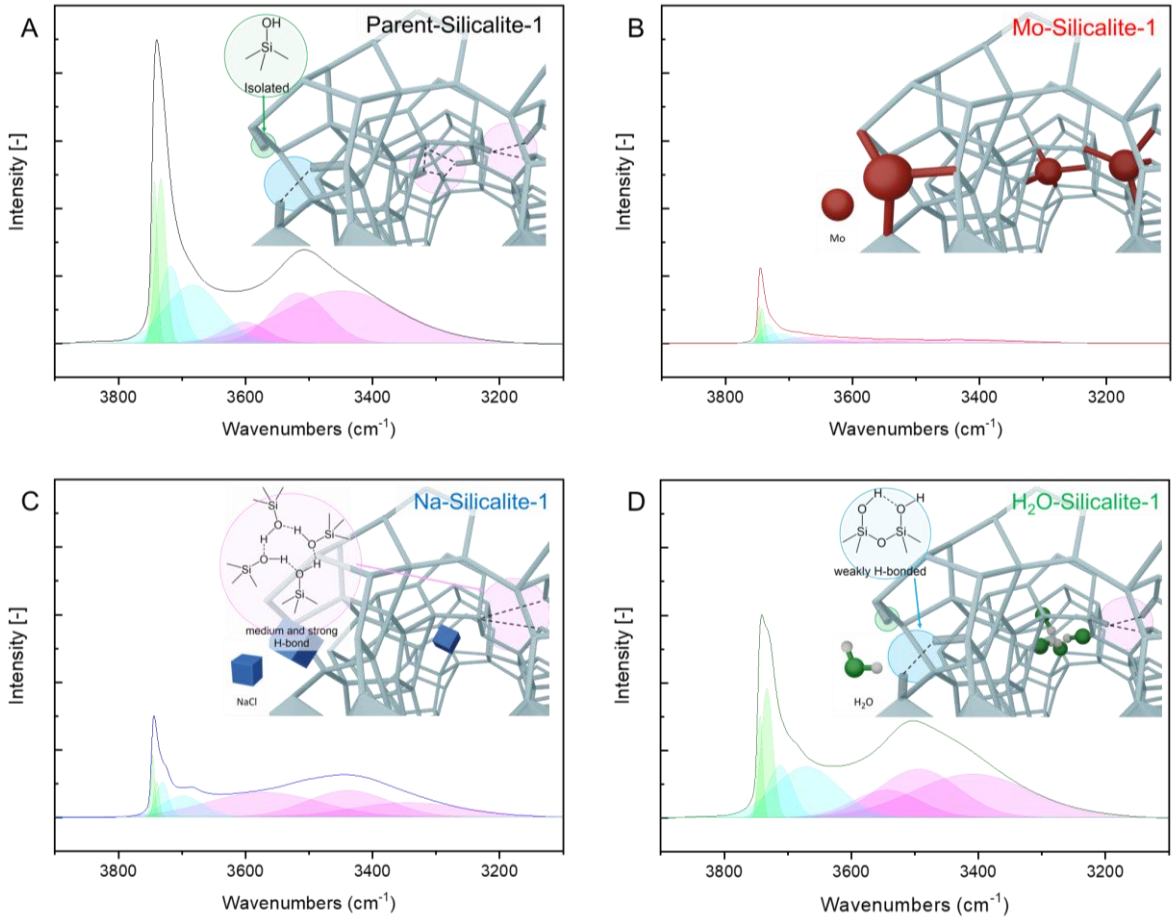

Figure 4. FTIR spectra with deconvoluted bands in the hydroxyl region (4000-3000 cm^{-1}) of (A) Parent-Silicalite-1, (B) Mo-Silicalite-1, (C) Na-Silicalite-1, and (D) H_2O-Silicalite-1 samples.

Based on the semi-quantitative analysis of normalized FTIR spectra (Figure 5,A), a 33% reduction in the isolated silanol groups and a 2% reduction in the strong hydrogen-bonded silanol groups were calculated after treatment of the Parent-Silicalite-1 sample with ultrapure water (**Figure 4D)**. Treatments with sodium molybdate and sodium chloride resulted in a 90% and 85% reduction of the isolated silanol groups, respectively, along with a 73% and 40% reduction in the strong hydrogen-bonded silanol groups for Mo-Silicalite-1 and Na-Silicalite-1 samples, respectively (**Figure 4B and C**).

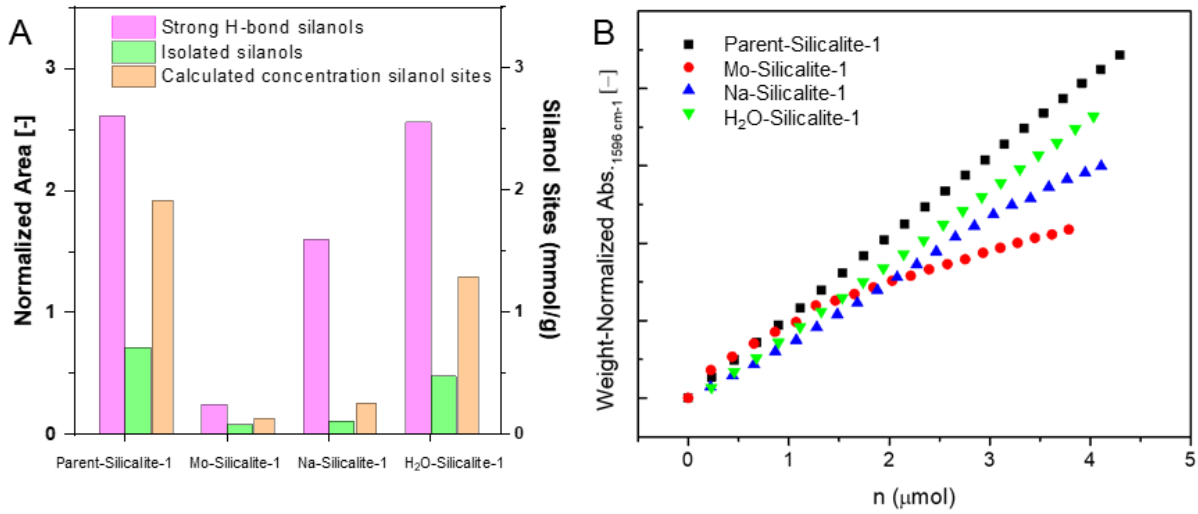

Figure 5. (A) Semi-quantitative comparison of the sum of the weight-normalized areas of the Gaussian functions underlying the medium and strong interactions in the region 3600-3200 cm^{-1} (purple), isolated silanols 3740-3735 cm^{-1} (green), and the quantitative concentration of isolated silanols measured at 1596 cm^{-1} in according to method reported elsewhere[30]. (B) Evaluation of the weight-normalized area related to the 8a stretching mode of silanols (1596 cm^{-1}) as a function of the molar increase of Py concentration.

Additionally, the silanol groups in the parent and post-treated samples were studied by FTIR of Py adsorbed (**Figure S.1)**. The FTIR spectra of the samples recorded after the adsorption of Py show five bands at 1597, 1577, 1492 and 1446 cm^{-1}, corresponding to the 8a, 8b, 19a and 19b normal modes of the CCN vibrations, respectively[31,32]. As the concentration of the Py increases, the weak 19a band at 1492 cm^{-1} corresponding to A1 symmetry becomes more pronounced. The band 19b (B2 symmetry) splits into two absorption bands at 1445 and 1433 cm^{-1} related to pi-type ring interactions of the physisorbed Py [31]. The band at 1597 cm^{-1} is associated with the 8a vibration mode, which is assigned to silanol groups bonded to Py. The Parent Silicalite-1 and H_2 O-Silicalite-1 samples show a linear increase in Py adsorption, while the Mo-Silicalite-1 and Na-Silicalite-1 samples reach a plateau at low Py concentrations of 1.5 and 3.5 μmol, respectively. Py associated with free silanol groups is desorbed as the temperature increases, leading to a reduction in the intensity of the 1446 cm^{-1} and 1597 cm^{-1} bands and a strengthening of bands in the hydroxyl region. The concentration of the SiOH groups was quantified by calculating the molar absorbance of Py at 1597 cm^{-1} for each sample (ε_{1595}= 0.25 ± 0.04 $cm^{-1}mol^{-1}$)[30] at 90 °C (**Figure S2**). The terminal silanol group concentration decreased by 93% and 87% for the Mo-Silicalite-1 and Na-Silicalite-1 samples, respectively (**Figure 6B**). This is further supported by the synchronous and asynchronous 2D-

COS evaluation of the FTIR data (**Figure 6**). A comparison of spectra for Na-Silicalite-1 and H_2 O-Silicalite-1 with the Parent-Silicalite-1, at incremental Py adsorption (0-4.1 μmol), shows that the bands at 1597, 1578, and 1445 cm^{-1} increase proportionally with Py concentration (**Figures S3** and **S4**). In the synchronous 2D-COS spectra for Mo-Silicalite-1 and Parent-Silicalite-1 (**Figure 6A**), a new adsorption band appears at 1489 cm^{-1} (**Figure 6B**).

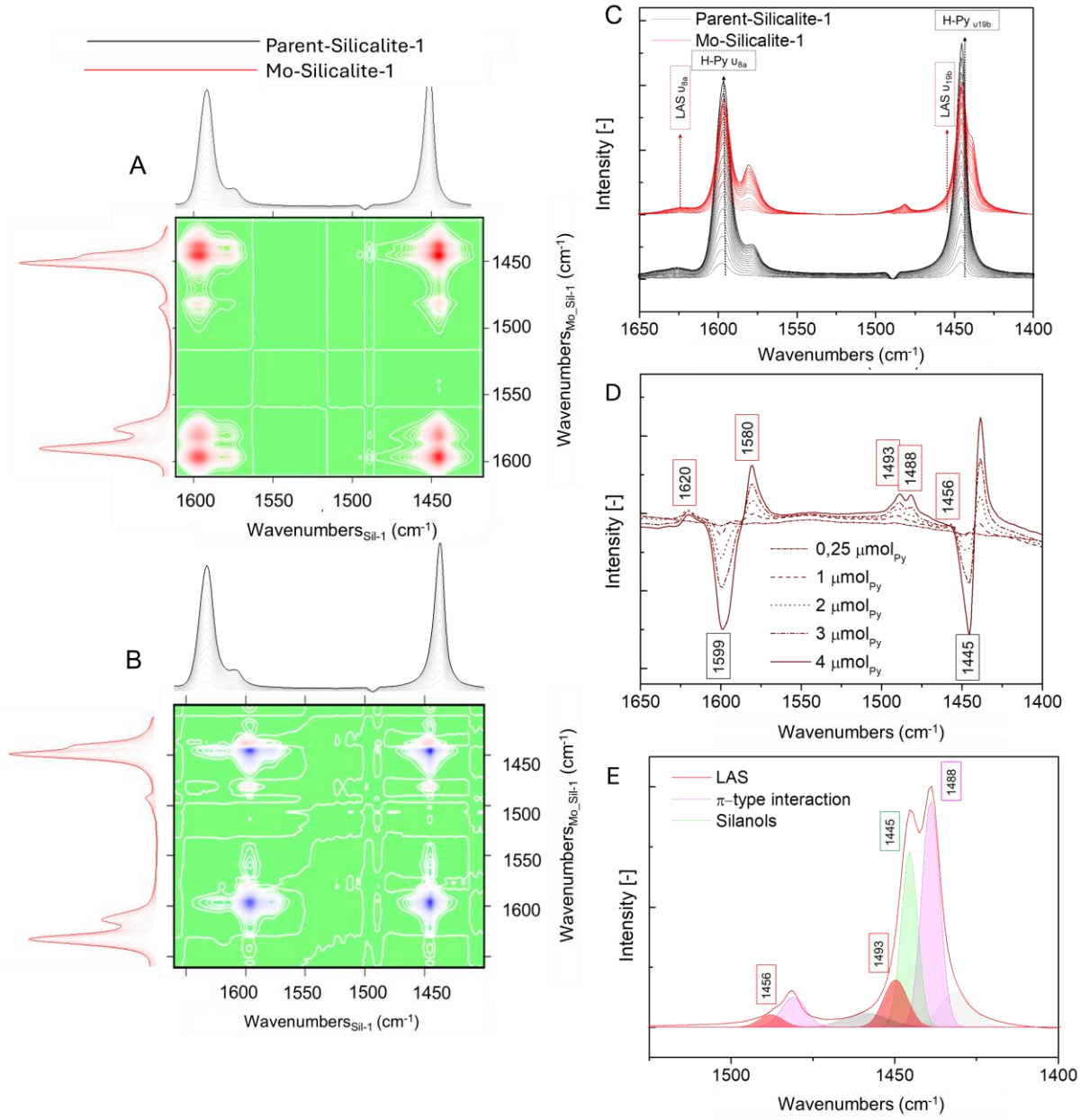

Figure 6. (A) Synchronous correlation and (B) asynchronous correlation in 2D COS (Two-Dimensional Correlation Spectroscopy) spectra of Mo-Silicalite-1 and Parent-Silicalite-1 samples in the 1650-1400 cm^{-1} range. (C) Direct comparison of the spectra of Mo-Silicalite-1 (in red) and Parent-Silicalite-1 (in black) after Py adsorption carried out dose-by-dose in the region 1650-1400 cm^{-1}. Subtraction of the normalized spectra of Mo-Silicalite-1 and Parent-Silicalite-1 for equal numbers of moles of Py adsorbed. (D) The positive peaks represent the component present in Mo-Silicalite-1 and absent in the Parent-Silicalite-1 sample. (E) Deconvolution of the

FTIR spectra in the region of 1550-1400 cm^{-1} for sample Mo-Silicalite-1 after Py adsorption at 25 °C (2.022 torr).

The adsorption of Py is directly related to the concentration of silanol groups in the samples. The Py adsorbed on Parent-Silicalite-1 resulted in very intense absorption bands at 1446, 1580 and 1597 cm^{-1}, along with weaker bands 1495 and 1622 cm^{-1} due to the high concentration of silanol groups (**Figure 7**). The latter bands correspond to the 8a and 19a stretching mode of the weak Lewis acid centers[33] and tend to disappear after heating the Parent-Silicalite-1 sample to temperatures above 90 °C under vacuum. For the Mo-Silicalite-1 sample, these bands become more pronounced due to the presence of Lewis acid sites (**Figure 7C**) and exhibit a slight shift to lower frequencies. By subtracting the normalized spectra for equal numbers of moles of Py (**Figures 7D** and **S5**), it becomes clear that the increase in these bands is proportional to the emergence of a peak at 1456 cm^{-1}, which represents the 8a stretching mode of Lewis sites (5.31 μmol g^{-1}; ε_{1456}= 2.22 ± 0.04 cm^{-1} mol^{-1})[34]. Unlike other samples, these peaks show significant stability even at 120 °C (**Figure S1**), suggesting a greater strength of these sites compared to pure silica samples reported in the literature[35].

Based on the Py adsorption measurements performed on activated samples, it is possible to assess the condensation of silanol groups and the resulting formation of strained, unsymmetrical siloxane bonds. This is evidenced by the appearance of a band at 895 cm^{-1}, which corresponds to the presence of unsymmetrical siloxane bonds (unsymmetrical siloxane bond) [36].

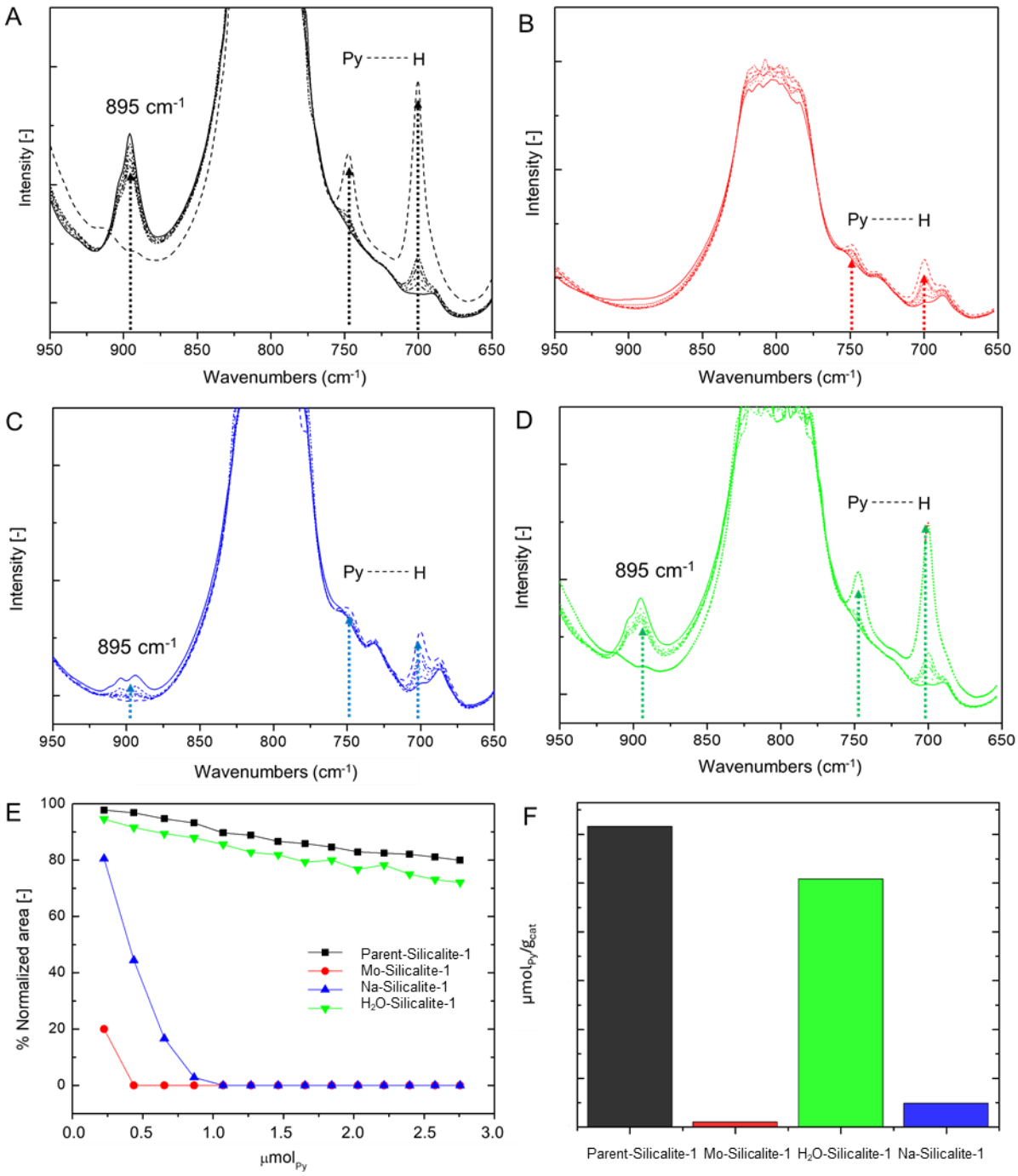

Figure 7. FTIR spectra after Py adsorption carried out dose-by-dose on (A) Parent-Silicalite-1, (B) Mo-Silicalite-1, (C) Na-Silicalite-1, and (D) H_2O-Silicalite-1; the solid line shows the spectrum after activation, the dot- lines show the spectra with 1.07, 2.02, 2.93 and 3.78 µmol Py and the dash-line shows the spectrum after saturation (2.052 torr). (E) Reduction of the normalized area of the peak at 891 cm^{-1} (%) *vs* the number of moles of Py introduced into the system. (F) Py amount required for complete elimination of the peak at 895 cm^{-1} representing the structural defects for samples Parent-Silicalite-1, Mo-Silicalite-1, Na-Silicalite-1, and H_2O-Silicalite-1.

The intensity of the band at 895 cm^{-1} ascribed to the number of structural defects in the samples decreased upon the introduction of Py molecule. The reduction and eventual disappearance of this band indicate that the highly strained Si-O-Si bridges present in the Parent-Silicalite-1 sample break, facilitating the formation of SiOH and hydroxyl groups bonded to Py. This observation allows for the estimation of the quantity of highly deformed Si-O-Si bridges in the samples, as illustrated in **Figure 7 E-F**. The Parent-Silicalite-1 and H_2O-Silicalite-1 samples exhibit a significant number of defects, requiring 13.55 and 11.18 μmol of Py, respectively, to fully saturate the unsymmetrical bridging sites. In contrast, the Mo-Silicalite-1 sample appears to be free of defects, and for Na-Silicalite-1, only 1.07 μmol of Py is needed to saturate all the siloxane sites.

Therefore, while molybdenum contributes to the removal of a considerable amount of isolated and weakly hydrogen-bonded silanol groups through its insertion into the zeolite framework, as stated in our earlier studies, sodium plays a distinct role in condensing open bridges within the zeolite framework. The removal of silanol groups is facilitated by their electrostatic interaction with Na^+ , which promotes the formation of siloxy groups (SiO^-). These siloxy groups subsequently condense with adjacent SiOH groups, releasing water molecules during the calcination process.

Conclusions

In this work, the removal of silanol groups using three post-synthesis approaches on nanosized Silicalite-1 sample applying sodium molybdate, sodium chloride and ultrapure water was explored. The post-synthesis treatments with sodium molybdate and sodium chloride induced an orthorhombic-to-monoclinic phase transition, leading to a 0.26% increase in unit cell volume compared to the sample treated with water. XRD, ^{29}Si NMR and $\{^1H\}^{29}Si$ CPMAS NMR analyses demonstrated that the post-treatments resulted in varying degrees of angular distribution for the tetrahedral sites and the removal of silanol groups, in the following order: sodium molybdate > sodium chloride > ultrapure water. The reduction in silanol group concentration was further confirmed by FTIR spectroscopy, showing a clear decrease in the same order. Although the concentration of molybdenum incorporated into the zeolite framework was relatively low (0.26 wt%, corresponding to 5.31 μmol g^{-1} of Lewis acid sites), sodium also played an active role in these processes. The post-synthesis treatment with sodium chloride produced effects similar to those observed with sodium molybdate, leading to the removal of approximately 90% of the silanol groups in Na-Silicalite-1,

comparable to the 98% removal in Mo-Silicalite-1. In contrast, the treatment with ultrapure water (H_2O-Silicalite-1) removed only about 20% of the silanol groups. This work provides new insights into the reactivity and condensation of silanol groups in high-silica nanosized zeolites, highlighting their relationship with flexibility and the hydrogen bond networks established within their porous structures.

Acknowledgments

Funded by the European Union (ERC, ZEOLIghT, 101054004). Views and opinions expressed are however those of the author(s) only and do not necessarily reflect those of the European Union or the European Research Council. Neither the European Union nor the granting authority can be held responsible for them. The support of the Centre for Zeolites and Nanoporous Materials, Label of Excellence, Normandy Region (CLEAR) is acknowledged.

Data availability statement

The data that support the findings of this study are available from authors upon request.

Declaration of interest statement

The authors declare that they have no known competing financial interests or personal relationships that could have appeared to influence the work reported in this article.

References

(1) Guisnet, M.; Gilson, J. Catalytic Science Series, Vol. 3 Zeolites for Cleaner Technologies. *Focus on Catalysts* **2003**, *2003*.

(2) Dib, E.; Mineva, T.; Veron, E.; Sarou-Kanian, V.; Fayon, F.; Alonso, B. ZSM-5 Zeolite: Complete al Bond Connectivity and Implications on Structure Formation from Solid-State NMR and Quantum Chemistry Calculations. *Journal of Physical Chemistry Letters* **2018**, *9* (1), 19–24. https://doi.org/10.1021/acs.jpclett.7b03050.

(3) Van Koningsveld, H.; Van Bekkum, H.; Jansen, J. C. On the Location and Disorder of the Tetrapropylammonium (TPA) Ion in Zeolite ZSM- 5 with Improved Framework Accuracy. *Acta Crystallographica Section B* **1987**, *43* (2), 127–132. https://doi.org/10.1107/S0108768187098173.

(4) van Koningsveld, H.; Jansen, J. C.; van Bekkum, H. The Monoclinic Framework Structure of Zeolite H-ZSM-5. Comparison with the Orthorhombic Framework of as-Synthesized ZSM-5. *Zeolites* **1990**, *10* (4), 235–242. https://doi.org/10.1016/0144-2449(94)90134-1.

(5) Yokomori, Y.; Idaka, S. The Structure of TPA-ZSM-5 with Si/Al=23. *Microporous and Mesoporous Materials* **1999**, *28* (3), 405–413. https://doi.org/10.1016/S1387-1811(98)00311-4.

(6) Sivadinarayana, C.; Choudhary, V. R.; Vetrivel, R.; Ganapathy, S. Characterization of Silicon Sites in Monoclinic Zeolite ZSM-5 Using 29Si Magic Angle Spinning (MAS) Nuclear Magnetic Resonance (NMR) and Molecular Modelling. *Solid State Nucl Magn Reson* **1998**, *13* (3), 175–182. https://doi.org/10.1016/S0926-2040(98)00079-4.

(7) Marra, G. L.; Artioli, G.; Fitch, A. N.; Milanesio, M.; Lamberti, C. Orthorhombic to Monoclinic Phase Transition in High-Ti-Loaded TS-1: An Attempt to Locate Ti in the MFI Framework by Low Temperature XRD. *Microporous and Mesoporous Materials* **2000**, *40* (1–3), 85–94. https://doi.org/10.1016/S1387-1811(00)00244-4.

(8) Mentzen, B. F.; Gelin, P. The Silicalite/p-Xylene System : Part I — Flexibility of the MFI Framework and Sorption Mechanism Observed during p-Xylene Pore-Filling by X-Ray Powder Diffraction at Room Temperature. *Mater Res Bull* **1995**, *30* (3), 373–380. https://doi.org/10.1016/0025-5408(95)00003-8.

(9) Fyfe, C. A.; Grondey, H.; Feng, Y.; Kokotailo, G. T. Investigation of the Three-Dimensional Si□O□Si Connectivities in the Monoclinic Form of Zeolite ZSM-5 by Two-Dimensional 29Si INADEQUATE Experiments. *Chem Phys Lett* **1990**, *173* (2–3), 211–215. https://doi.org/10.1016/0009-2614(90)80080-W.

(10) Fyfe, C. A.; Joseph Lee, J. S.; Cranswick, L. M. D.; Swainson, I. Powder Neutron Diffraction Determination of the Structure of the O-Xylene/Zeolite ZSM-5 Complex. *Microporous and Mesoporous Materials* **2008**, *112* (1–3), 299–307. https://doi.org/10.1016/J.MICROMESO.2007.10.026.

(11) Fyfe, C. A.; Lee, J. S. J. Solid-State NMR Determination of the Zeolite ZSM-5/Ortho-Xylene Host-Guest Crystal Structure. *Journal of Physical Chemistry C* **2008**, *112* (2), 500–513. https://doi.org/10.1021/JP074816Z/SUPPL_FILE/JP074816ZSI20070921_063403.PDF.

(12) Fyfe, C. A.; Brouwer, D. H. Solid-State NMR and X-Ray Diffraction Structural Investigations of the p-Nitroaniline/ZSM-5 Complex. *Microporous and Mesoporous Materials* **2000**, *39* (1–2), 291–305. https://doi.org/10.1016/S1387-1811(00)00210-9.

(13) Fyfe, C. A.; Grondey, H.; Feng, Y.; Kokotailo, G. T. Natural-Abundance Two-Dimensional 29Si MAS NMR Investigation of the Three-Dimensional Bonding Connectivities in the Zeolite Catalyst ZSM-5. *J Am Chem Soc* **1990**, *112* (24), 8812–8820. https://doi.org/10.1021/JA00180A024/ASSET/JA00180A024.FP.PNG_V03.

(14) Fabbiani, M.; Al-Nahari, S.; Piveteau, L.; Dib, E.; Veremeienko, V.; Gaje, A.; Dumitrescu, D. G.; Gaveau, P.; Mineva, T.; Massiot, D.; Van Der Lee, A.; Haines, J.; Alonso, B. Host-Guest Silicalite-1 Zeolites: Correlated Disorder and Phase Transition Inhibition by a Small Guest Modification. *Chemistry of Materials* **2022**, *34* (1), 366–387. https://doi.org/10.1021/acs.chemmater.1c03721.

(15) Medeiros-Costa, I. C.; Dib, E.; Dubray, F.; Moldovan, S.; Gilson, J. P.; Dath, J. P.; Nesterenko, N.; Aleksandrov, H. A.; Vayssilov, G. N.; Mintova, S. Unraveling the Effect of Silanol Defects on the Insertion of Single-Site Mo in the MFI Zeolite Framework. *Inorg Chem* **2022**, *61* (3), 1418–1425. https://doi.org/10.1021/acs.inorgchem.1c03076.

(16) Grand, J.; Talapaneni, S. N.; Vicente, A.; Fernandez, C.; DIb, E.; Aleksandrov, H. A.; Vayssilov, G. N.; Retoux, R.; Boullay, P.; Gilson, J. P.; Valtchev, V.; Mintova, S. One-Pot Synthesis of Silanol-Free Nanosized MFI Zeolite. *Nature Materials 2017 16:10* **2017**, *16* (10), 1010–1015. https://doi.org/10.1038/nmat4941.

(17) Prodinger, S.; Derewinski, M. A.; Vjunov, A.; Burton, S. D.; Arslan, I.; Lercher, J. A. Improving Stability of Zeolites in Aqueous Phase via Selective Removal of Structural Defects. *Journal of American Chemical Society* **2016**, *138* (13), 4408–4415. https://doi.org/10.1021/jacs.5b12785.

(18) Janiszewska, E.; Macario, A.; Wilk, J.; Aloise, A.; Kowalak, S.; Nagy, J. B.; Giordano, G. The Role of the Defect Groups on the Silicalite-1 Zeolite Catalytic Behavior. *Microporous and Mesoporous Materials* **2013**, *182*, 220–228. https://doi.org/10.1016/j.micromeso.2012.12.013.

(19) Bordiga, S.; Roggero, I.; Ugliengo, P.; Zecchina, A.; Bolis, V.; Artioli, G.; Buzzoni, R.; Marra, G.; Rivetti, F.; Spano, G.; Lamberti, C. Characterisation of Defective Silicalites f. *Journal of the Chemical Society, Dalton Transactions* **2000**, No. 21, 3921–3929. https://doi.org/10.1039/b004794p.

(20) Medeiros-Costa, I. C.; Dib, E.; Nesterenko, N.; Dath, J. P.; Gilson, J. P.; Mintova, S. Silanol Defect Engineering and Healing in Zeolites: Opportunities to Fine-Tune Their Properties and Performances. *Chem Soc Rev* **2021**, *50* (19), 11156–11179. https://doi.org/10.1039/d1cs00395j.

(21) Vayssilov, G. N.; Aleksandrov, H. A.; Dib, E.; Costa, I. M.; Nesterenko, N.; Mintova, S. Superacidity and Spectral Signatures of Hydroxyl Groups in Zeolites. *Microporous and Mesoporous Materials* **2022**, *343* (August), 112144. https://doi.org/10.1016/j.micromeso.2022.112144.

(22) Resasco, D. E.; Crossley, S. P.; Wang, B.; White, J. L. Interaction of Water with Zeolites: A Review. *Catal Rev Sci Eng* **2021**, *63* (2), 302–362. https://doi.org/10.1080/01614940.2021.1948301.

(23) Dib, E.; Costa, I. M.; Vayssilov, G. N.; Aleksandrov, H. A.; Mintova, S. Complex H-Bonded Silanol Network in Zeolites Revealed by IR and NMR Spectroscopy Combined with DFT Calculations. *J Mater Chem A Mater* **2021**, *9* (48), 27347–27352. https://doi.org/10.1039/D1TA06908J.

(24) Medeiros-Costa, I. C.; Dib, E.; Dubray, F.; Moldovan, S.; Gilson, J. P.; Dath, J. P.; Nesterenko, N.; Aleksandrov, H. A.; Vayssilov, G. N.; Mintova, S. Unraveling the Effect of Silanol Defects on the Insertion of Single-Site Mo in the MFI Zeolite Framework. *Inorg Chem* **2022**, *61* (3), 1418–1425. https://doi.org/10.1021/acs.inorgchem.1c03076.

(25) Konnov, S. V.; Dubray, F.; Clatworthy, E. B.; Kouvatas, C.; Gilson, J. P.; Dath, J. P.; Minoux, D.; Aquino, C.; Valtchev, V.; Moldovan, S.; Koneti, S.; Nesterenko, N.; Mintova, S. Novel Strategy for the Synthesis of Ultra-Stable Single-Site Mo-ZSM-5 Zeolite Nanocrystals. *Angewandte Chemie International Edition* **2020**, *59* (44), 19553–19560. https://doi.org/10.1002/ANIE.202006524.

(26) Guo, R.; Zhang, X.; He, A. Q.; Zhang, F.; Li, Q. B.; Zhang, Z. Y.; Tauler, R.; Yu, Z. Q.; Morita, S.; Xu, Y. Z.; Noda, I.; Ozaki, Y.; Wu, J. G. A Novel Systematic Absence of Cross Peaks-Based 2D-COS Approach for Bilinear Data. *Spectrochim Acta A Mol Biomol Spectrosc* **2019**, *220*, 117103. https://doi.org/10.1016/J.SAA.2019.05.008.

(27) Toby, B. H.; Von Dreele, R. B. GSAS-II: The Genesis of a Modern Open-Source All Purpose Crystallography Software Package. *urn:issn:0021-8898* **2013**, *46* (2), 544–549. https://doi.org/10.1107/S0021889813003531.

(28) Engelhardt, G.; Michel, Dieter. *High-Resolution Solid-State NMR of Silicates and Zeolites*; Wiley, 1987.

(29) Bordiga, S.; Ugliengo, P.; Damin, A.; Lamberti, C.; Spoto, G.; Zecchina, A.; Spanò, G.; Buzzoni, R.; Dalloro, L. Hydroxyls Nests in Defective Silicalites and Strained Structures Derived upon Dehydroxylation : Vibrational Properties and Theoretical Modelling. *Top Catal* **2001**, *15* (1), 43–52. https://doi.org/10.1023/A:1009019829376.

(30) Ramírez, A.; Lopez, B. L.; Sierra, L. Study of the Acidic Sites and Their Modifications in Mesoporous Silica Synthesized in Acidic Medium under Quiescent Conditions. *Journal of Physical Chemistry B* **2003**, *107* (35), 9275–9280. https://doi.org/10.1021/JP0351472.

(31) Velthoen, M. E. Z.; Nab, S.; Weckhuysen, B. M. Probing Acid Sites in Solid Catalysts with Pyridine UV-Vis Spectroscopy. *Physical Chemistry Chemical Physics* **2018**, *20* (33), 21647–21659. https://doi.org/10.1039/C8CP03991G.

(32) Kline, C. H.; Turkevich, J. The Vibrational Spectrum of Pyridine and the Thermodynamic Properties of Pyridine Vapors. *J Chem Phys* **1944**, *12* (7), 300–309. https://doi.org/10.1063/1.1723943.

(33) Rajagopal, S.; Marzari, J. A.; Miranda, R. Silica-Alumina-Supported Mo Oxide Catalysts: Genesis and Demise of Brønsted-Lewis Acidity. *J Catal* **1995**, *151* (1), 192–203. https://doi.org/10.1006/JCAT.1995.1021.

(34) Emeis, C. A. Determination of Integrated Molar Extinction Coefficients for Infrared Absorption Bands of Pyridine Adsorbed on Solid Acid Catalysts. *J Catal* **1993**, *141* (2), 347–354. https://doi.org/10.1006/JCAT.1993.1145.

(35) Óvári, L.; Solymosi, F. Determination of Acidic Centers on Supported Mo2C Catalysts. *J Mol Catal A Chem* **2004**, *207* (1), 35–40. https://doi.org/10.1016/S1381-1169(03)00469-2.

(36) Zhao, X. S.; Lu, G. Q.; Whittaker, A. K.; Millar, G. J.; Zhu, H. Y. Comprehensive Study of Surface Chemistry of MCM-41 Using 29 Si CP/MAS NMR, FTIR, Pyridine-TPD, and TGA. **1997**. https://doi.org/10.1021/JP971366.